Preprints of the 19th World Congress
The International Federation of Automatic Control
Cape Town, South Africa. August 24-29, 2014

Model-Based Estimation of Large-Scale Interconnected Power Systems with Moving PHEV Loads

Pardis Khayyer*, and Ümit Özgüner*

** Department of Electrical and Computer Engineering and Center for Automotive Research (CAR), The Ohio State University, Columbus, OH, 43210 USA*
(email: {khayyer.1},{ozguner.1}@osu.edu)

Abstract: Power system dynamics change because of variations in distribution circuit, performance of power generation and behavior of load. An estimation of these dynamical behaviors can be achieved using mathematical models. Interconnected systems with shared state variables require specific models to demonstrate the influence of parameter variations on all areas. Estimation is particularly difficult when the system is influenced by random load variations such as moving plug-in hybrid electric vehicle (PHEV) loads. This paper introduces a new model-based estimation technique designed for large scale interconnected systems. This high performance state estimation demonstrated an accurate effective, real-time and computationally efficient approach. State estimations and their transient behavior were successfully obtained for a power system with random loads as high as 327 level-1 charging vehicles at various storage device charge levels.

1. INTRODUCTION

Perturbations in Large-scale interconnected systems (e.g. electric power systems) are mainly the result of varying operating conditions, system dynamics, and failures. Parameter variations due to fault and noise in large-scale interconnected systems significantly affect their dynamic behavior. State estimation of the integrated systems requires an effective, real-time and computationally efficient technique. When the system parameters change as a result of system perturbations, the dynamic behavior can be represented as a new model. Multiple of these models can configure a set of possible scenarios.

In Multiple model adaptive estimation (MMAE) technique, banks of Kalman filters run in parallel to detect dynamic variations of the system. Kalman filters are weighted by the likelihood of model correctness using probability density functions (Tjahyadi, Fangpo & Sammut, 2004; Maybeck & Hanlon, 1995; Menke & Maybeck, 1995, Maybeck, 1999).

The probability evaluator, which generates the probability weights, operates based on measurement residuals. This method is a well-known technique and is used for variety of applications (Hanlon & Maybeck, 2000; Tjahyadi, Fangpo & Sammut, 2004; Boskovic & Mehra, 1999; Cezayirli & Ciliz, 2004; Izadian & Famouri, 2010; Martin, Schneider & Smith, 1987; Izadian, Khayyer & Famouri, 2009).

In this paper, a state estimation technique for large-scale interconnected overlapping systems is presented using multiple model adaptive estimation technique. The Kalman filters are designed for modeling of noise and interconnected system parameter variations. The main parameter variation is considered as the load imposed by moving PHEVs on the power grid (Tuffner, Kintner-Meyer, 2011), (Kintner-Meyer, Nguyen, Jin, Balducci, Secrest, 2010), (Khayyer, Ozguner, 2013). The estimation technique is used in solving the problem of frequency control of a large-scale interconnected power system. Various types of disturbances are applied as load. The benchmark power system selected for studies is a two-area power system with a tie-line interconnection (Khayyer, Ozguner, 2014). Several power generation units including wind and diesel backed by a battery storage unit exist in area 1. In area 2, a micro-hydro power generation unit feed loads. The tie-line interconnection between two systems and its parameters (e.g. transferred power) directly affect the power system operation, and more importantly, the power transient stability.

2. SYSTEM DYNAMICS

As stated earlier, the system studied in this paper is an interconnected two-area generation unit. Area 1 includes a hybrid wind-diesel backed by a battery storage that is connected to the network through a droop-based inverter, and area 2 is a micro-hydro generation unit that uses synchronous generators. Dynamic components of the overall system are linearized around the system's nominal operating point for stability analysis (Kundur, 1994). Linear model of power system components are obtained in this section.

2.1 Storage System Dynamics

Figure 1 illustrates the overall schematic and small signal model of the Battery Energy Storage System (BESS). Power electronic droop (Guerrero, Berbel, Matas, et al.,2007), (Guerrero, Vasquez, Matas, 2009) , (Guerrero, Chandorkar, Lee, Loh, 2013) , (Guerrero, Loh, Lee, Chandorkar, 2013) and battery SOC level are taken into account in this storage modelling mainly for battery inverters in the system.

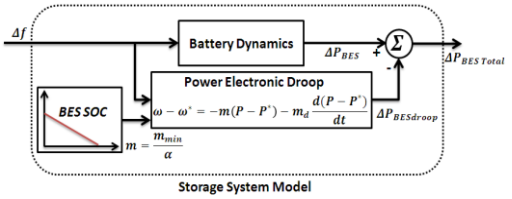

Figure 1. Block diagram of battery energy storage modelling

In this model, battery dynamics is presented as a first order transfer function (Kottick, Blau, 1993), (Lee, Wang, 2008), (Bhongade, Tyagi, Gupta, 2011).

$$G_{BESS}(s) = \frac{K_{BESS}}{1+sT_{BESS}} \quad (1)$$

where K_{BESS} is the plant gain and T_{BESS} is the time constant of storage system. Droop consideration reduces battery power contribution when the SOC level is low. The droop modeling is shown in equation (2) (Guerrero, Vasquez, Matas, 2009) , (Guerrero, Chandorkar, Lee, Loh, 2013), (Guerrero, Loh, Lee, Chandorkar, 2013).

$$\omega = \omega^* - m(P - P^*) - m_d \frac{d(P-P^*)}{dt} \quad . \quad (2)$$

where ω is the frequency of inverter and ω^* is the frequency at no-load. $(P - P^*)$ represents $\Delta P_{BESdroop}$ in this system and m_d and m represent droop coefficients. Variable droop coefficient is adjusted according to the battery SOC and is calculated as (Guerrero, Vasquez, Matas, 2009),

$$m = \frac{m_{min}}{\alpha} \quad (3)$$

where m_{min} is the default minimum droop coefficient and α is equal to 1 when battery is fully charged (SOC=100%) and is equal to a lower saturation bound when battery is empty.

2.2 Overall two area system model

Overall generation system is made up of two sub-area generation systems. Small-signal block diagram of the first sub-area (hybrid generation system of wind, battery, and diesel) is presented in Figure 2 (Bhatti, Al-Ademi, Bansal, 1997), (Bansal, Bhatti, 2008).

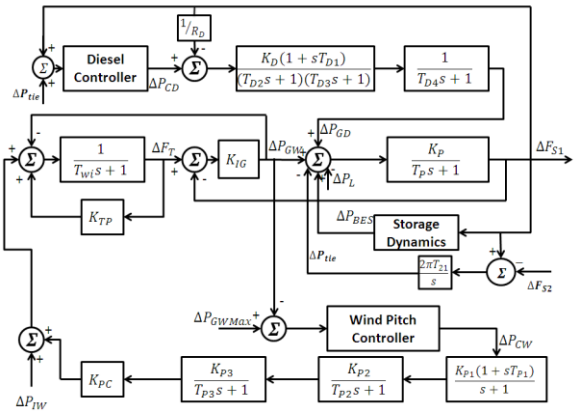

Figure 2. Block diagram of hybrid generation system (first generation area)

The second-generation sub-area is considered as a micro-hydro generation unit. Figure 3 illustrates small-signal dynamic model of the micro-hydro generation unit (Kundur, 1994).

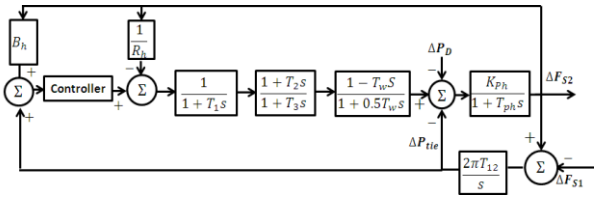

Figure 3. Dynamic model of the hydro generation unit (Kundur, 1994)

Considering the overall system as the hybrid wind-battery-diesel and micro-hydro system, state variables of the overall system are:

$$X = [\Delta F_{s1}, \Delta P_{GD}, \Delta X_{ED1}, \Delta X_{ED2}, \Delta F_T, \Delta X_{PC1}, \Delta X_{PC2}, \Delta X_{PC3}, \Delta P_{BES}, \Delta P_{BESdroop}, \Delta P_{tie}, \Delta F_{s2}, \Delta P_{GH}, \Delta P_{RH}, \Delta X_{EH}, \Delta P_{refH}]$$

where ΔF_{s1} is frequency of the first area (hybrid system), ΔP_{GD} is fluctuation in the diesel generator power, ΔX_{ED1}, ΔX_{ED2} are diesel generator governor valves position, ΔF_T is the wind turbine frequency, $\Delta X_{PC1}, \Delta X_{PC2}, \Delta X_{PC3}$ are wind turbine pitch control actuators, ΔP_{BES} is the battery power, $\Delta P_{BESdroop}$ is the battery droop power, ΔP_{tie} is the tie-line power between the two areas, ΔF_{s2} is frequency of the second area (micro hydro unit), ΔP_{GH} is the fluctuation in turbine generated power, ΔP_{RH} is the mechanical power from water flow, ΔX_{EH} is the hydro unit governor valve position and, ΔP_{refH} is the variable achieving integral control. The system has one shared (overlap) state variable (ΔP_{tie}) between two areas.

In large-scale power systems, where electric power generation is shared by two or more generators, speed of power generators directly influences active power flow. Therefore, disturbance in one generation area affects the voltage frequency in other areas. In such occasions, frequency is restored through droop control of power generation units (Boldea, 2005), (Xu, Mathur, Jiang, et al, 1998) also known as Automatic Generation Control (AGC) of alternating current (AC) power system (Kundur, 1994), (Bergen, Vittal, 1999). In a disturbance event, electrical frequency of an interconnection must be maintained close to its nominal level (e.g. 60 Hz). Area control error (ACE) is considered as

$$ACE_i = B_i \Delta F_i + \sum_{j=1}^{m} a_{ij} \Delta P_{tie,ij} \quad , \quad (4)$$

where B_i is the frequency bias factor of area i, ΔF_i is the area frequency error from nominal value (60 Hz), a_{ij} is the operator depending on per unit base difference of two subsystems, and $\Delta P_{tie,ij}$ is the tie-line power interchange between areas i and j. For detailed model dynamics, refer to (Khayyer, 2013) and (Khayyer, Ozguner, 2014).

One of the major applications of overlapping decompositions is in Automatic Generation Control (AGC) (Kundur, 1994), (Bergen, Vittal, 1999) of alternating current (AC) power system. In overlapping decomposition technique, shared state variables between subsystems is considered in design of controller. In the next section, state estimation technique for large-scale interconnected overlapping systems is presented using multiple model adaptive estimation technique.

3. LARGE-SCALE POWER SYSTEM PHEV LOAD ESTIMATION

In field implementation of control systems, the original system S is subject to system and measurement noise, which can be represented as:

$$S: \begin{cases} \dot{x} = Ax + Bu + Lw \\ y = Cx + v \end{cases}, \quad (5)$$

where $x \in \mathbb{R}^n, u \in \mathbb{R}^m$ and $y \in \mathbb{R}^l$ are states, input and output vectors of system S, L is the input noise matrix $(n \times s)$, $(s < n)$, w is the zero mean system noise, and v is zero mean output measurement noise. The system noise variance, Q_c, and measurement noise variance, R_c, have zero correlation, i.e. independent values. In large-scale overlapping system estimation, first the system is expanded into a large space and then decomposed into disjoint subsystems (Iftar, Ozguner, 1987), (Iftar, Ozguner, 1989), (Iftar, Ozguner, 1998), (Iftar, Ozguner, 1990), (Siljak, 1991). The expanded system is expressed as:

$$\tilde{S}: \begin{cases} \dot{\tilde{x}} = \tilde{A}\tilde{x} + \tilde{B}\tilde{u} \\ \tilde{y} = \tilde{C}\tilde{x} \end{cases}, \quad (6)$$

where $\tilde{x} \in \mathbb{R}^{\tilde{n}}, \tilde{u} \in \mathbb{R}^{\tilde{m}}$ and $\tilde{y} \in \mathbb{R}^{\tilde{l}}$ as states, input and output vectors of system $\tilde{S}$. It is assumed that $n \le \tilde{n}$, $m \le \tilde{m}$ and, $l \le \tilde{l}$. For $i = 1{:}N$, N subsystems in the expanded space are presented as:

$$\tilde{S}_i: \begin{cases} \dot{\tilde{x}}_i = \tilde{A}_i\tilde{x}_i + \tilde{B}_i\tilde{u}_i + \tilde{L}_i w_i \\ \tilde{y}_i = \tilde{C}_i\tilde{x}_i + v_i \end{cases} \quad (7)$$
$$for\ i = 1, \dots, N$$

For detailed extension transformations refer to (Iftar, Ozguner, 1987), (Iftar, Ozguner, 1989), (Iftar, Ozguner, 1998), (Iftar, Ozguner, 1990), (Siljak, 1991).

The expanded subsystem, $\tilde{S}$, is decomposed into disjoint subsystems which Kalman based state estimation is designed for. Kalman filter minimizes the estimation error covariance, defined as follows:

$$P = \lim_{t \to \infty} E[(x - \hat{x})(x - \hat{x})^T], \quad (8)$$

where P is *a posteriori* error covariance matrix. Algebraic Riccati equation (8) generates the optimum covariance matrix as follows:

$$\dot{P} = -PC^T R_c^{-1} CP + AP + PA^T + Q_c. \quad (9)$$

Observable time invariant or slowly time variant systems generate a steady state (finite) covariance matrix (Simon, 2006 and Izadian, Khayyer & Famouri, 2009).

For the system studied in this paper, the Kalman filter estimation is formulated within the context of Inclusion principle (Khayyer, 2013). In this case, Riccati equations are solved in the expanded space for each subsystem and multiple model Kalman based estimators are derived for each subsystem (Tjahyadi, Fangpo & Sammut, 2004; Maybeck & Hanlon, 1995; Menke & Maybeck, 1995, Maybeck, 1999). Therefore, state estimated model j for each subsystem i of the expanded system is presented as:

$$\dot{\hat{\tilde{x}}}_{ij} = \tilde{A}_i\hat{\tilde{x}}_{ij} + \tilde{B}_i\tilde{u}_{ij} + \tilde{H}_{ij}\left[\tilde{y}_i - \tilde{C}_i\hat{\tilde{x}}_{ij}\right]. \quad (10)$$
$$for\ i = 1, \dots, N\ and\ j = 1, \dots, M$$

Based on system real-time measurement, the model correctness weights are assigned by a probability evaluator to each multiple model. Figure 4 presents the overlapping multiple model adaptive estimation scheme for decupled expanded subsystem i with M Kalman based estimated models. Detailed mathematical formulation and theories of this technique are represented at (Khayyer, 2013). In the next section, this technique is applied for a two-area power system experiencing variations in PHEV load level.

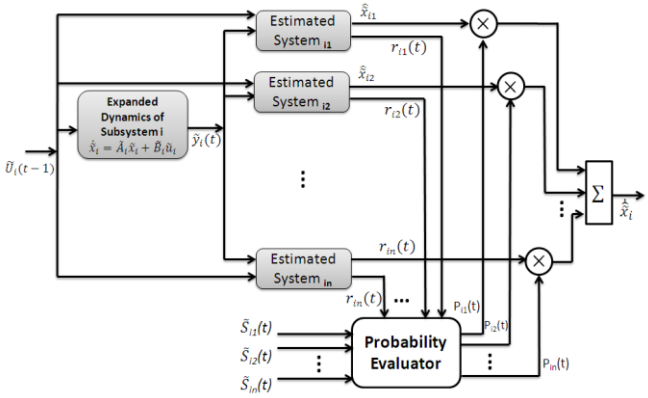

Figure 4. Overlapping multiple model adaptive estimation scheme for decupled expanded subsystem i with M Kalman based estimated models.

4. CASE STUDIES

Disturbances applied to the system is in the form of load variation uncertainties e.g. PHEV load migration from one area to the other. To consider real-world implementations, inherently existing measurement noise and system noise were applied to all the system operation scenarios.

To decouple the large-scale interconnected systems, the overlapping decomposition theory was applied. Decoupled sub-systems consist of several models of the desired operating conditions. A system contingency estimator using multiple model adaptive estimator was used to generate the probabilities associated to each subsystem's contingency models. Table 1 presents a summary of the four case studies presented in this paper.

Table 1. Case studies for subsystems I and II, Base Power 100 MW

Case Study	Subsystem I and II			
	Battery SOC	Moving Load Level/Factor	# PHEVs in Charge Level 1	# PHEVs in Charge Level 2
1	90%	1	155	31
2	35%	1		
3	90%	2	327	66
4	35%	2		

In the first case, system state estimation for different scenarios is performed when the size of moving loads varies and the stationary battery is charged up to 90%. In first three steps of operation scenario, the loads of subsystem I are varied without any effect on subsystem II (varying under two scenarios). However, the loads are considered moving from subsystem I to subsystem II in operation scenarios 4 and 5. Overall relation between subsystems I & II load variation scenarios are presented in Figure 5.

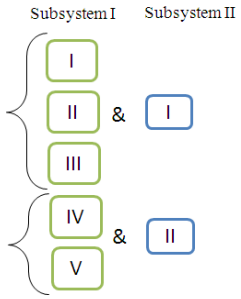

Figure 5. Relation between subsystems I & II load variations scenarios

Figure 6 shows the probabilities associated to each operation scenario. As the figure demonstrates, the shift in probabilities are accurate to detect the appropriate system operation. A mismatch occurred at the transition from model 3 to model 5. However, the system is quickly recovered and the probability is set to the right system.

Figure 7 demonstrates the probabilities of subsystem II. As the figure shows, the probabilities are associated to the correct model in each contingency. In the first part of the graph, although the moving loads are not shifted to subsystem II, the effect of load change was observed on this subsystem operation through a tie-line. When the moving loads migrated to the subsystem II, the probabilities shifted to the second model with smooth transition.

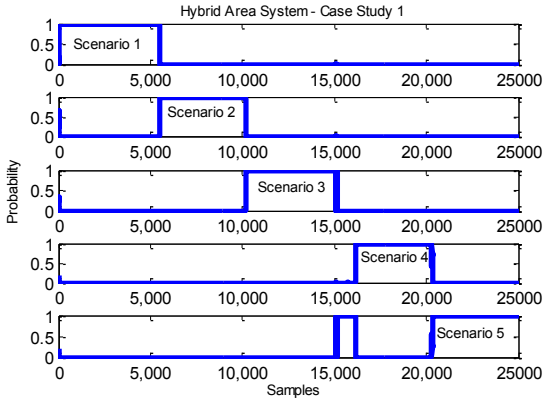

Figure 6. Probability values associated with multiple models in subsystem I in case 1.

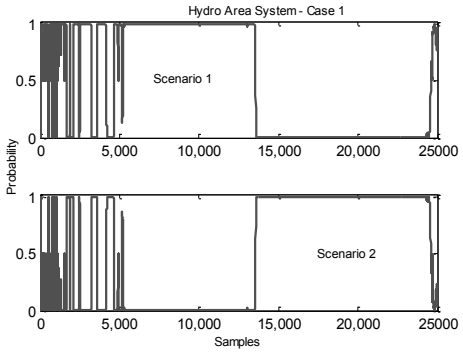

Figure 7. Probability values associated with multiple models in subsystem II. The models show the load shift in case 1.

In the second case, system state estimation for different scenarios is performed when the size of moving loads changed with a minimally charged battery (SOC of 35%). In first three steps of operation scenario, the loads of subsystem I were varied without any effect on subsystem II. However, the loads were considered moving from subsystem I to subsystem II in operation scenarios 4 and 5. Figure 8 shows the probabilities associated to each operation scenario. As the figure demonstrates, the shift in probabilities accurately detected the appropriate system operation. A mismatch occurred at the transition from model 3 to model 4. However, the system was quickly recovered and the probability was set to the right system. Figure 9 demonstrates the probabilities of subsystem II. As the figure shows, the probabilities were associated to the correct model. Similar to case 1, in the first part of the graph, although the moving loads were not shifted to the hydro power plant, the effect of load change was observed on the system operation as the two systems were connected through a tie-line. When the moving loads migrated to the subsystem II, the probabilities shifted to the second model. Some transitions were observed in the second model. The transitions might have been generated from the fact that the dynamics of two models were similar. The battery was depleted and the moving load level matched with that of observed in subsystem II.

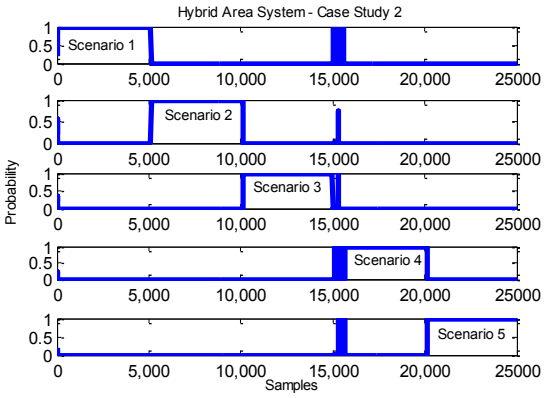

Figure 8. Probability values associated with multiple models in subsystem I in case 2.

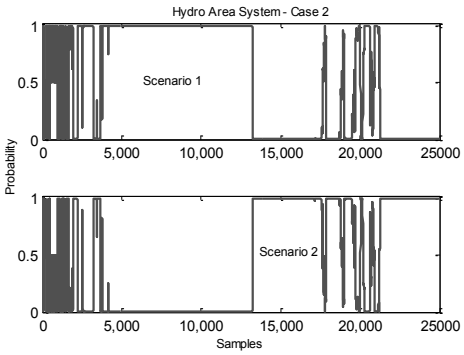

Figure 9. Probability values associated with multiple models in subsystem II. The models show the load shift in case 2.

In order to evaluate the system performance under higher load levels, a load factor of 2 was considered for case studies 3 and 4. System conditions of case study 3 was similar to case 1 with the exception that now the load level for case 3 was doubled compared to case 1. Similar relationship was true between cases 2 and 4. In order to obtain the desired level of load migration, the noise input matrix L was directly scaled.

In this case, the system transient moving loads were

limited to 472 kW in addition to the base load. The system experienced a ±472 kW load change and was required to control the frequency drop or increase as a result of the load change. This level of load transient translated to 327 PHEVs at charging level 1 or 66 PHEVs at charge level 2 for a base power of 100 MW as shown in Table 1. Subsystems I and II experienced this load change differently. In first three steps of operation scenario, the loads of subsystem I were varied without any effect on subsystem II. However, the loads were considered moving from subsystem I to subsystem II in operation scenarios 4 and 5.

Figure 10 shows the probabilities associated to each operation scenario. As the figure demonstrates, the shift in probabilities were accurate to detect the appropriate system operation. A transient mismatch occurred at the transition from model 3 to model 4. However, the system was quickly recovered and the probability was set to the correct system.

Figure 11 demonstrates the probabilities of subsystem II. As the figure shows, the probabilities were associated to the correct model. In the first part of the graph, as the moving load variation level was increased in subsystem I, the effect of load change was observed for longer time on the first part of the probabilities in subsystem II. The load power was shared through tie-line from subsystem II to subsystem I. When the moving loads migrated to the subsystem II, the probabilities shifted to the second model with smooth transition.

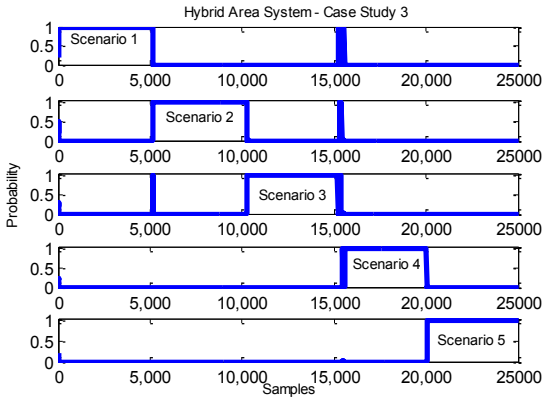

Figure 10. Probability values associated with multiple models in subsystem I in case 3.

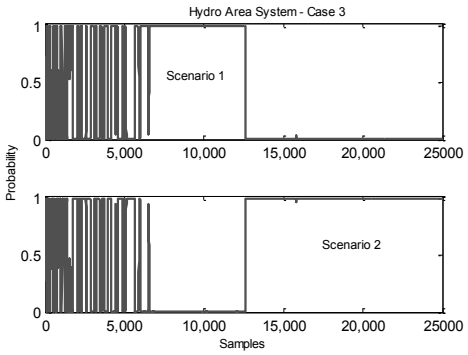

Figure 11. Probability values associated with multiple models in subsystem II. The models show the load shift in case 3.

As stated earlier, case study 4 is similar to case 2 except that in case 4 the load factor was increased to 2. Figure 12 shows the probabilities associated to each operation scenario for the first area. As the figure demonstrates, the shift in probabilities were accurate to detect the appropriate system operation. Except for a small delay in transition from model 2 to 3, no mismatch occurred at the transition among models.

Figure 13 demonstrates the probabilities of subsystem II. As the figure shows, the probabilities were associated to the correct model. In the first part of the graph, although the moving loads were not shifted to the hydro power plant, the effect of load change was observed on the system operation as the two systems were connected through a tie-line. When the moving loads migrated to the subsystem II, the probabilities shifted to the second model. Some transitions were observed in the second model mainly due to higher noise levels.

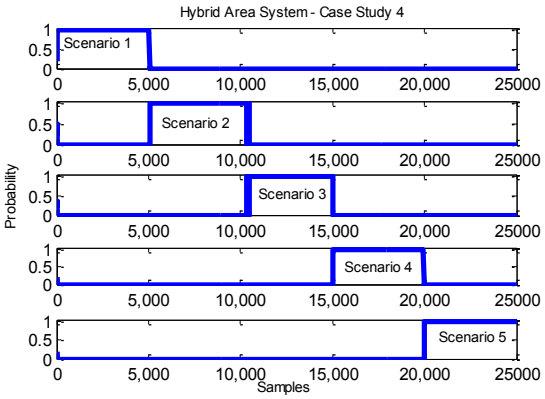

Figure 12. Probability values associated with multiple models in subsystem I in case 4

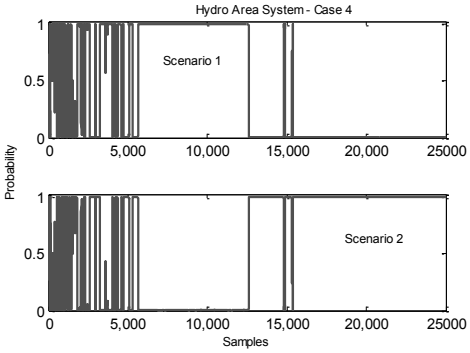

Figure 13. Probability values associated with multiple models in subsystem II. The models show the load shift in case 4.

As it was shown in all four case studies, correct model representation of the system under different load levels can be detected using the MMAE technique for the decentralized subsystems. Small transients associated with model detection were mainly the result of system noise level and system dynamics.

5. CONCLUSION

In this paper, multiple model adaptive estimation technique was implemented for state space estimation of large-scale interconnected power systems. In a two-area power system, load power variation was considered as noise in the system and was modeled to a high extent using Kalman filters. MMAE provided a platform in which the desired modes of operation and operating conditions was properly estimated.

ACKNOWLEDGEMENTS

This research was supported by U.S. DOE Graduate Automotive Technology Education (GATE) Center of Excellence, DE FG26 05NT42616. Discussions with Dr. David Schoenwald of Sandia National Laboratories are gratefully acknowledged.

REFERENCES

Bansal, R. C., Bhatti, T. S. (2008). *Small signal analysis of isolated hybrid power system: reactive power and frequency control analysis*. Alpha Science International Ltd.

Bergen, A. R., Vittal, V. (1999). *Power systems analysis*. Prentice Hall.

Bhatti, T.S., Al-Ademi, A.A.F., Bansal, N.K. (1997). Load frequency control of isolated wind diesel hybrid power systems. *Energy Conversion and Management*, 38(9), (pp. 829–837).

Bhongade, S., Tyagi, B., Gupta, H.O. (2011). Automatic generation control scheme based wind power generating system. *2011 Annual IEEE India Conference* (INDICON).

Boldea, I. (2005). *Synchronous generators* (The Electric Generators Handbook). CRC Press.

Boskovic, J. D., Mehra, R. K. (1999). Stable multiple model adaptive flight control for accommodation of a large class of control effector failures. *American Control Conference*, 3, (pp. 1920-1924).

Cezayirli, A., Ciliz, K. (2004). Multiple model based adaptive control of a DC motor under load changes. In proceedings of *IEEE International Conference on Mechatronics*, (pp. 328-333).

Guerrero, J. M., Berbel, N., Matas, J. Sosa, J. L., de Vicuna, L. G. (2007). Droop control method with virtual output impedance for parallel operation of uninterruptible power supply systems in a microgrid. *Twenty Second Annual IEEE Applied Power Electronics Conference*, APEC.

Guerrero, J. M., Vasquez, J. C., Matas, J., Castilla, M., de Vicuna, L. G. (2009). Control strategy for flexible microgrid based on parallel line-interactive UPS systems. *IEEE Transactions on Industrial Electronics*, 56(3), (pp.726-736).

Guerrero, J. M., Chandorkar, M., Lee, T. L., Loh, P. C. (2013). Advanced control architectures for intelligent microgrids—part I: Decentralized and hierarchical control. *IEEE Transactions on Industrial Electronics*, 60(4), (pp.1254-1262).

Guerrero, J. M., Loh, P. C., Lee, T. L., Chandorkar, M. (2013). Advanced control architectures for intelligent microgrids—part II: Power quality, energy storage, and AC/DC microgrids. *IEEE Transactions on Industrial Electronics*, 60(4), (pp.1263-1270).

Hanlon, P. D., Maybeck, P. S. (2000). Multiple-model adaptive estimation using a residual correlation Kalman filter bank. *IEEE Transactions on Aerospace and Electronic Systems*, 36(2), (pp. 393-406).

Iftar, A., Ozguner, U. (1987). Local LQG/LTR controller design for decentralized systems. *IEEE Transactions on Automatic Control*, 32(10), (pp. 926-930).

Iftar, A., Ozguner, U. (1989). An optimal control approach to the decentralized robust servomechanism problem. *IEEE Transactions on Automatic Control*, 34(12), (pp. 1268-1271).

Iftar, A., Ozguner, U. (1990). Contractible controller design and optimal control with state and input inclusion. *Automatica*, 26(3), (pp. 593-597).

Iftar, A., Ozguner, U. (1998). Overlapping decompositions, expansions, contractions, and stability of hybrid systems. *IEEE Transactions on Automatic Control*, 43(8), (pp.1040-1055).

Izadian, A., Khayyer, P., Famouri, P. (2009). Fault diagnosis of time-varying parameter systems with application in MEMS LCRs. *IEEE Transactions on Industrial Electronics*, 56(4), (pp. 973-978).

Izadian, A., Famouri, P. (2010). Fault Diagnosis of MEMS Lateral Comb Resonators Using Multiple-Model Adaptive Estimators. *IEEE Transactions on Control Systems Technology*, 18(5), (pp. 1233-1240).

Kintner-Meyer, M., Nguyen, T. B., Jin, C., Balducci, P., Secrest, T. (2010). Impact Assessment of Plug-in Hybrid Vehicles on the U.S. Power Grid. *The 25th World Battery, Hybrid and Fuel Cell Electric Vehicle Symposium & Exhibition.*

Khayyer, P. (2013). Multiple model based estimation and control in large-scale interconnected systems. *PhD Dissertation*, Department of Electrical and Computer Engineering, The Ohio State University, Columbus, OH.

Khayyer, P., Ozguner, U. (2013). Decentralized control of smart grid with fixed and moving loads. In Proc. of *IEEE Power and Energy Conference at Illinois* (PECI) 2013.

Khayyer, P., Ozguner, U. (2014). Decentralized control of large-scale storage-based renewable energy systems. *IEEE Transactions on Smart Grid*, Accepted.

Kottick, D., Blau, M., Edelstein, D. (1993). Battery energy storage for frequency regulation in an island power system. *IEEE Transactions on Energy Conversion*, 8(3), (pp.455-459)

Kundur, P. (1994). *Power system stability and control*, McGraw-Hill, Inc.

Lee, D., Wang, L. (2008). Small-signal stability analysis of an autonomous hybrid renewable energy power generation/energy storage system part I: Time-domain simulations. *IEEE Transactions on Energy Conversion*, 23(1), (pp.311-320).

Martin, J. F., Schneider, A. M., Smith, N. T. (1987). Multiple-model adaptive control of blood pressure using Sodium Nitroprusside. *IEEE Transactions on Biomedical Engineering*, 34(8), (pp. 603-611).

Maybeck, P. S., Hanlon, P. D. (1995). Performance enhancement of a multiple model adaptive estimator. *IEEE Transactions on Aerospace and Electronic Systems*, 31(4), (pp. 1240-1254).

Maybeck, P. (1999). Multiple model adaptive algorithms for detecting and compensating sensor and actuator/surface failures in aircraft flight control systems. *International Journal of Robust and Nonlinear Control*, 9, (pp. 1051-1070).

Menke, T. E., Maybeck, P. S. (1995). Sensor/actuator failure detection in the Vista F-16 by multiple model adaptive estimation. *IEEE Transactions on Aerospace and Electronic Systems*, 31(4), (pp. 1218-1229).

Siljak, D. D. (1991). *Decentralized control of complex systems*. Academic Press (Siljak, 1991).

Simon D. (2006). *Optimal state estimation: Kalman, H Infinity, and nonlinear approaches*. Wiley-Interscience.

Tjahyadi, H., Fangpo, H., Sammut, K. (2004). Vibration control of a cantilever beam using multiple model adaptive control. *American Control Conference*, 3, (pp. 2907-2908).

Tuffner, F. K., Kintner-Meyer, M. (2011). Using electric vehicles to mitigate imbalance requirements associated with an increased penetration of wind generation. *IEEE Power and Energy Society General Meeting.*

Xu, X., Mathur, R. M., Jiang, J., Rogers, G. J., Kundur, P. (1998). Modeling of generators and their controls in power system simulations using singular perturbations. *IEEE Transactions on Power Systems*, 13(1), (pp.109-114).